Nuclear Instruments and Methods in Physics Research A 780 (2015) 100–106

Contents lists available at ScienceDirect

Nuclear Instruments and Methods in Physics Research A

journal homepage: www.elsevier.com/locate/nima

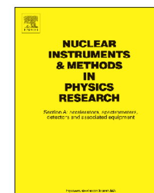

Reliable cool-down of GridPix detectors for cryogenic applications

R. Schön [a,*], J. Schmitz [b], S. Smits [b], Y. Bilevych [c], N. van Bakel [a]

[a] National Institute for Subatomic Physics Nikhef, Science Park 105, 1098XG Amsterdam, The Netherlands
[b] MESA+ Institute for Nanotechnology, University of Twente, P.O. Box 217, 7500AE Enschede, The Netherlands
[c] Physics Institute, University of Bonn, Nußallee 12, 53115 Bonn, Germany

ARTICLE INFO

Article history:
Received 21 November 2014
Received in revised form
19 January 2015
Accepted 20 January 2015
Available online 29 January 2015

Keywords:
GridPix
SU-8
Micro-pattern gaseous detector
InGrid
Liquid xenon
Cryogenics

ABSTRACT

In this paper we present thermal cycling experiments of GridPix radiation imaging detectors, in view of a potential application in a cryogenic experiment. The robustness of the GridPix detector is studied for various grid designs, as well as various mechanical and thermal surroundings. The grid design variations had insignificant effect on the grid strength. A low cool-down rate as well as good thermal contact are crucial for the durability of the grid. Further, additional strengthening at the grid edges proved necessary to maintain the integrity of the structure during thermal cycling, which was done using globtop adhesive. The combination of these measures led to 100% survival rate after thermal cycling down to $-130\,^{\circ}$C.

© 2015 Elsevier B.V. All rights reserved.

1. Introduction

The GridPix detector is a type of micro-pattern gaseous detector produced by microfabricating a Micromegas grid on top of a 2D pixel readout chip such as Medipix2 or Timepix [1–4]. It offers high-precision imaging of ionizing radiation in two or three dimensions. Micromegas fabrication with microtechnology offers high geometrical precision, high-purity materials and the possibility to mass-produce in existing clean room facilities [5]. In recent years the GridPix detector has come under consideration for weakly interacting massive particle (WIMP) search experiments involving dual-phase noble gas detectors within the R&D programme of the DARWIN (dark matter WIMP search with noble liquids) consortium [6].

To establish the viability of the GridPix option in these experiments, three questions are to be answered: Can the detector be cooled down repetitively without degrading its mechanical properties? Can we reach sufficient gas gain to detect single electrons? Can the electronics operate at cryogenic temperatures of $T_{\ell \mathrm{Ar}} = -186\,^{\circ}$C and $T_{\ell \mathrm{Xe}} = -110\,^{\circ}$C? For a discussion of the second and third question we refer to [7,8], respectively. In this paper we address the first question. We present experimental studies on thermal cycles of a variety of GridPix prototypes, embedded in various thermal environments, and show finite-element-method (FEM) simulations of the mechanical behaviour of the detector during cool-down.

2. Limitations of GridPix at low temperatures

The GridPix detector consists of a silicon microchip fabricated in standard CMOS (Timepix), a few-micrometer thick layer of high-ohmic material (silicon-rich silicon nitride, SiRN), insulating support pillars made of SU-8 photoresist material measuring 50 μm in height, and a 1 μm thick grid made of pure aluminium with holes of 38 μm diameter. In the central region of the GridPix structure, a periodic pattern of pillars physically connects the grid with the microchip, see Fig. 1. At the edges, the grid should be better confined to avoid curling and to suppress sparks due to local field enhancement. Large rectangular SU-8 support-ridges are normally positioned along the edges for that reason. It is however necessary to make periodic interruptions in these support ridges, so-called strain relief gaps, to prevent rupture of the SU-8 material during fabrication [9] and to improve the dissolution of not cross-linked SU-8.

In previous works, the adhesion strength of this material stack was studied under various fabrication conditions and after storage in a high humidity environment [10]. The study showed a clear moisture sensitivity and a strong dependence of adhesion on the details in the fabrication process.

It can be expected that a GridPix detector with poor adhesion properties in the layer stack will delaminate upon thermal cycling, as a result of the different thermal expansion coefficients (CTE) of the used materials. The suspended aluminium grid may wrinkle or tear under thermal cycling, as the thicker and stiffer silicon substrate dictates the physical dimensions of the structure at all temperatures.

* Corresponding author.
E-mail address: rolfs@nikhef.nl (R. Schön).

http://dx.doi.org/10.1016/j.nima.2015.01.075
0168-9002/© 2015 Elsevier B.V. All rights reserved.

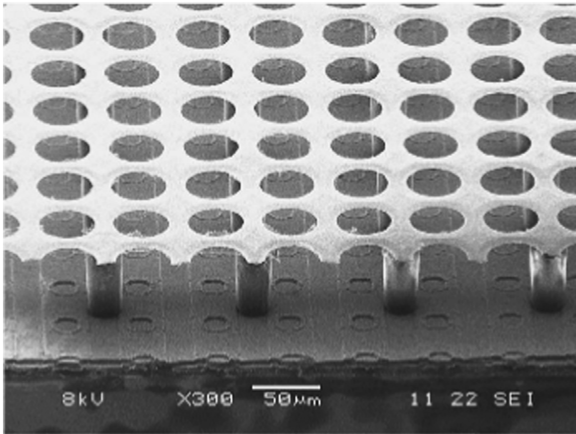

Fig. 1. Microscope picture showing the cross-section of a GridPix detector. A layer of silicon-rich silicon nitride protects the pixels of the Timepix readout chip against discharges. SU-8 pillars support the aluminium grid.

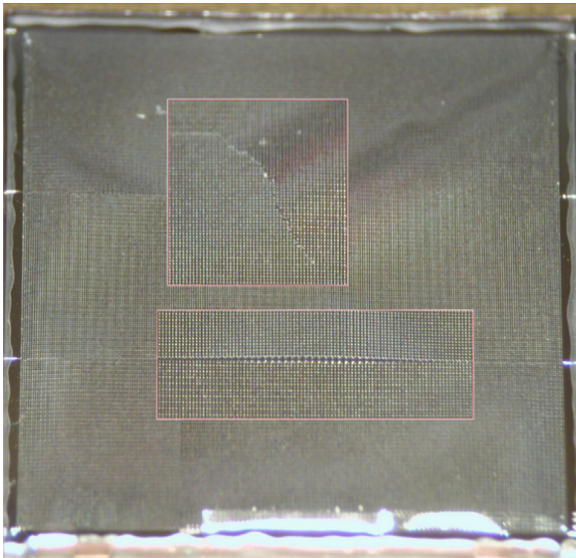

Fig. 2. Picture of the damaged grid after operating a GridPix inside the test cryostat of the ArDM experiment. During the cool-down of the argon gas inside the cryostat to −186 °C the detector was still working as expected. It was not until the filling the lower cryostat with liquid argon that the data suggested a breakage of the grid. The picture was taken after warming up and opening the cryostat.

A preliminary test of operating a GridPix in the prototype chamber of the Argon Dark Matter (ArDM) experiment [11] confirms this. After the exposure to dual-phase argon at −186 °C the grid showed severe damage, see Fig. 2. The ruptures in the grid start at the strain relief gaps of the SU-8 edge-support that are fixed to the substrate by globtop (epoxy).[1]

The robustness of GridPix detectors against thermal cycling was tested by controlled cool-down with liquid nitrogen to −130 °C. At this temperature, close to $T_{\ell Xe}$, the thermal stress is lower than at $T_{\ell Ar}$. First the samples were dried in a vessel in view of the moisture sensitivity mentioned above. The vessel was flushed with N_2 for 12 h at room temperature; then heated to 80 °C; then, after 30 min at 80 °C, cooled down and flushed in N_2 for several hours at room temperature.

The vessel was then inserted into a dewar with liquid nitrogen, well above the liquid surface. This provides cooling at a rate controlled to about 1 K/min by a heating element inside the vessel. The setup further includes thermometers near the samples and at the vessel bottom, see Fig. 3. The vessel is cooled to −130 °C and kept at this temperature for 30 min before gradually warming it up to room temperature.

The grids of two out of four devices survived the thermal cycle. The two other grids show similar damage: segments of the support ridge lifted off the protection layer. This is the result of the stress culminating at the borders as mentioned above. It points to an increased stress between the SU-8 and the SiRN layer in regions where the SU-8 structure is large. On the other hand, the two surviving samples indicate that a GridPix application in this cold environment is technically within reach.

3. SU-8 pattern modifications

Finite-element simulations[2] were conducted to investigate and visualize the effects of temperature cycling on the GridPix configuration. The thermal and mechanical properties of all employed materials as well as the thickness of the layers are listed in Table 1. We can assume that the silicon substrate imposes its lateral dimensions on the whole configuration thanks to its superior thickness. As clear from the table, the thermal expansion mismatch is highest at the SiRN–SU-8 interface, so this is a likely plane for delamination. A typical simulation result is shown in Fig. 4a. All thermal expansion mismatch tends to culminate at the edges, leading to a tendency of the aluminium to rupture starting from the edges, as observed in the aforementioned tests. Moreover, the peak stress values in the material stack shift from the grid to the substrate, see Fig. 4b, beneath the added support structures.

Based on the simulation results, several new designs were made with different SU-8 support features at the edge and in the pixel matrix area of the GridPix chip. The alternative edge designs and the reference are shown in Fig. 5. Further, bar structures were designed into the central region, aiming to form a more rigid construction which could lead to less aluminium excursion at the edges, see Fig. 6. The design sizes match the Timepix and Medipix readout chips [3,4].

Two dummy wafers with these modified designs and the reference GridPix design [10] were fabricated at Fraunhofer IZM Berlin to evaluate the differences between these patterns in terms of mechanical strength, thermal cycling robustness, and detector performance. Each wafer has 8 reference designs plus 9 instances of 11 modified designs (see [7] for further detail). The wafers have in common the silicon substrate, the SiRN protection layer of 2 μm thickness, the SU-8 structures and the aluminium grid, i.e. the integrated grid (InGrid) structure. One wafer, however, has an additional gold layer between the silicon substrate and the SiRN layer. This gold layer serves as anode to read out electrical signals in a setup discussed in Section 5.

4. Thermal cycling experiments of modified SU-8 patterns

The multiple samples allowed for a systematic study of the decisive factors influencing grid stability during thermal cycling. The following experimental conditions were varied:

- the SU-8 ridge structure (cf. Fig. 5);
- the SU-8 active area structure (cf. Fig. 6);
- samples with gold electrode and without;

[1] The used globtop is Dymax 9001-E-v3.1 UV/VIS adhesive [12].

[2] The simulations were performed with the Abaqus finite element analysis software [13].

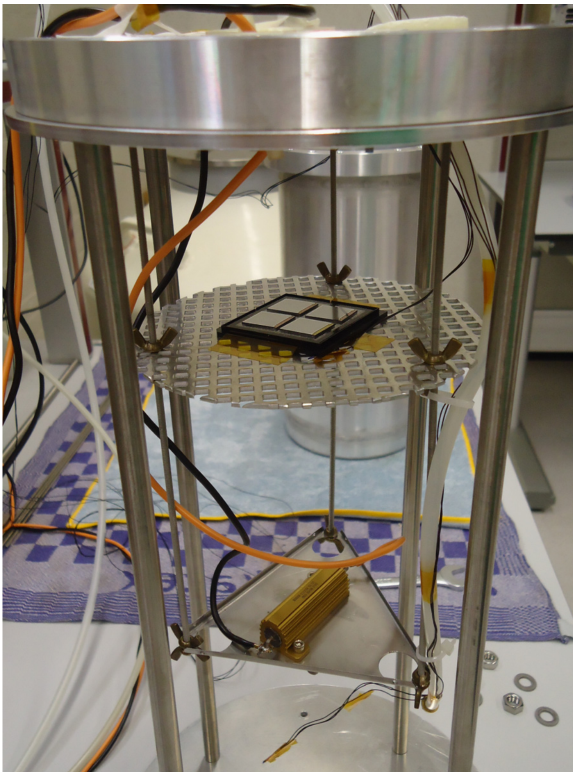

Fig. 3. Picture of the inside of the test vessel. The samples rest above the heating element that controls the temperature inside the vessel. A gas tube provides a constant flow of dry nitrogen to purge humidity. Two temperature sensors monitor the temperature of the samples and the vessel bottom.

Table 1
Thermal and mechanical properties of all employed materials used in the FEM simulations.

Property	Si	SiRN	SU-8	Al
Layer thickness (μm)	700	2–8	50	1
Therm. conductivity (W/(mK))	105	35	0.2	210
Density (g/cm^3)	2.33	3.2	1.19	2.7
Young's modulus (10^9 N/m^2)	112	300	4.02	68
Poisson's ratio	0.28	0.26	0.22	0.36
CTE (10^{-6}/K)	2.49	3.2	30	24
Specific heat (J/(kg K))	750	170	1200	900

- Tchips positioned on a metal block with cooling fins using heat-conductive paste, or loosely placed on thermally insulating plastic;
- globtop-coated grid edges (cf. Fig. 7) or uncoated edges.

The thermal cycle was always from room temperature to -130 °C and back, with ramp rates less than 1° per minute.

We found that the SU-8 designs and the presence of gold under the SiRN layer had no significant effect on the grid stability under thermal cycling. Mounting the chips to the cooling block using heat-conductive paste, as well as the administration of globtop, proved crucial. The results of two critical experiments are presented in Figs. 8 and 9. The first shows 20 samples after thermal cycling, five of which are unharmed. These five are exactly those with globtop edge reinforcement. Fig. 9 shows an experiment where all chips are globtop-reinforced and attached to the heat sink. All chips have remained intact.

We explain these results as follows. When the InGrid structure is confronted with a cold surroundings, the grid can cool quicker than the silicon wafer, because the latter is much thicker and has lower thermal conductivity. A large temperature difference can then build up between grid and chip, amplifying any thermal

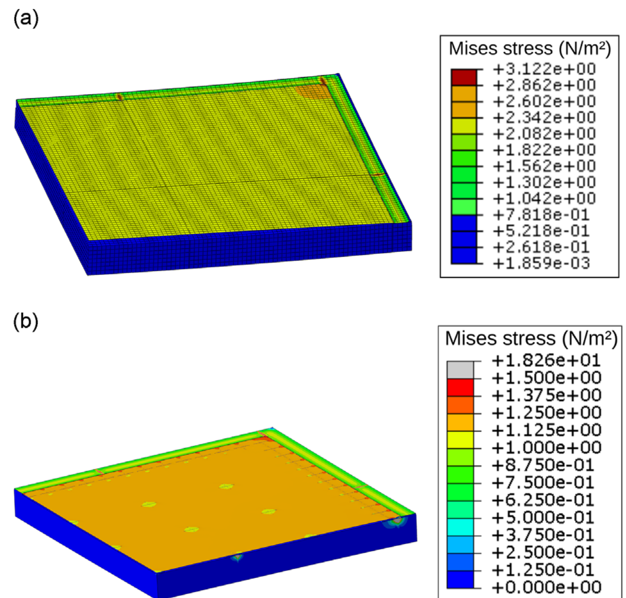

Fig. 4. FEM simulation results showing the van Mises stress as a result of temperature decrease. (a) The stress of shrinking aluminium grid culminates on the edges, particularly at the strain relief gaps of the SU-8 ridges. (b) Introducing cross structures (as shown in Fig. 6b) locally reduces the stress exerted by the grid and shifts the stress peaks into the silicon substrate. Hindering a translation of the grid reduces the stress on the grid edges. Note the different colour scale. (For interpretation of the references to colour in this figure caption, the reader is referred to the web version of this paper.)

expansion problems. Therefore a controlled cool-down requires the connection of the silicon chip to a kind of heat sink, besides a low-enough cool-down rate, to ensure that the silicon remains in thermal equilibrium with its surroundings.

A first, important conclusion is that the GridPix detector can sustain the whole thermal cycle. The heat-conductive paste improved the thermal conditions, i.e. reduced any thermal gradient. Nevertheless, the SU-8 dykes need to be fixed onto the chip edges by a thin film of globtop adhesive. None of the grid edge support arrangements displayed in Fig. 5 proved strong enough to keep the grid in place during these thermal cycles.

4.1. *Adhesion strength*

With a shear test tool (Dage ShearTool 4000) it was investigated whether the thermal cycle leads to deterioration of the adhesion of SU-8 to the underlying SiRN layer. The samples of the fourth batch were subjected to a shear test before and after the thermal cycling.

For this test we use two groups of alignment markers on the “bond pad” area of the InGrid chips, each group consisting of 4 of these markers. Fig. 10 shows an example of two chip corners with the alignment markers. For the adhesion test we use the 3 equal ones of each group. We measure the force required to delaminate the SU-8 markers from the underlying substrate. On most of the chips the markers rest on the gold anode layer. On three devices the SiRN layer extends further on the “bond pad” area, see also Fig. 10. To exclude the possible influence of local variations across the wafer we perform the shear test on every chip.

We obtain results of the shear force measurements before and after the thermal cycle for 15 samples.[3] The shear force required

[3] Note that we exclude the 5 chips with globtop around the grid edges. The low viscosity glue flowed around the SU-8 markers before curing with UV light, artificially increasing the required shear force.

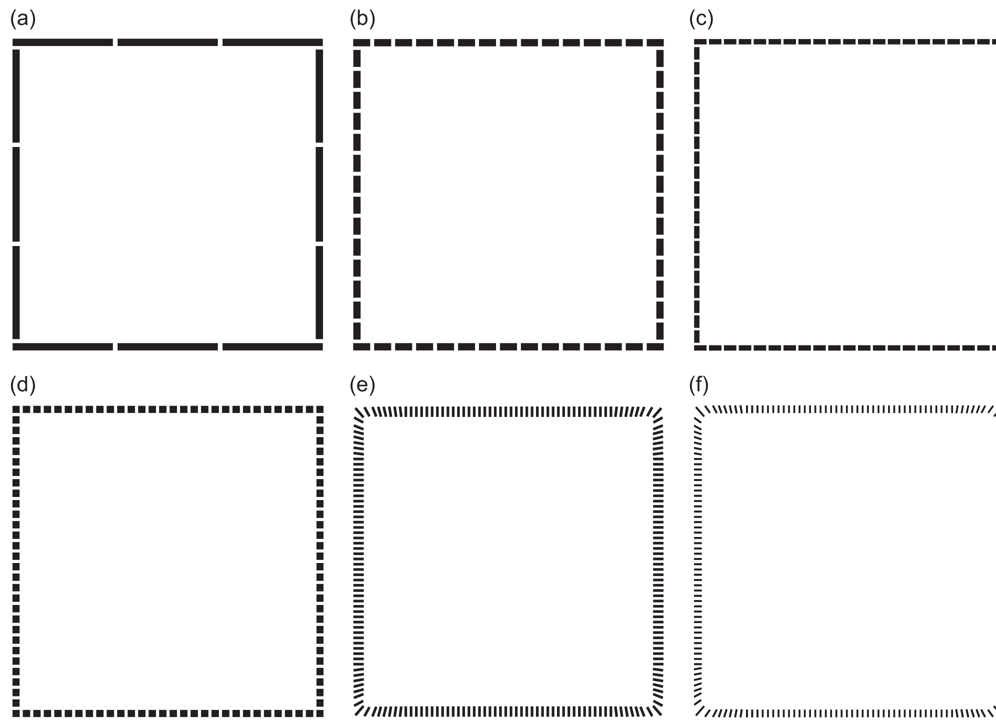

Fig. 5. Simplified sketches of SU-8 ridge structures as in the current design (a) and to reduce the lateral stress along the chip's edges (b)–(f).

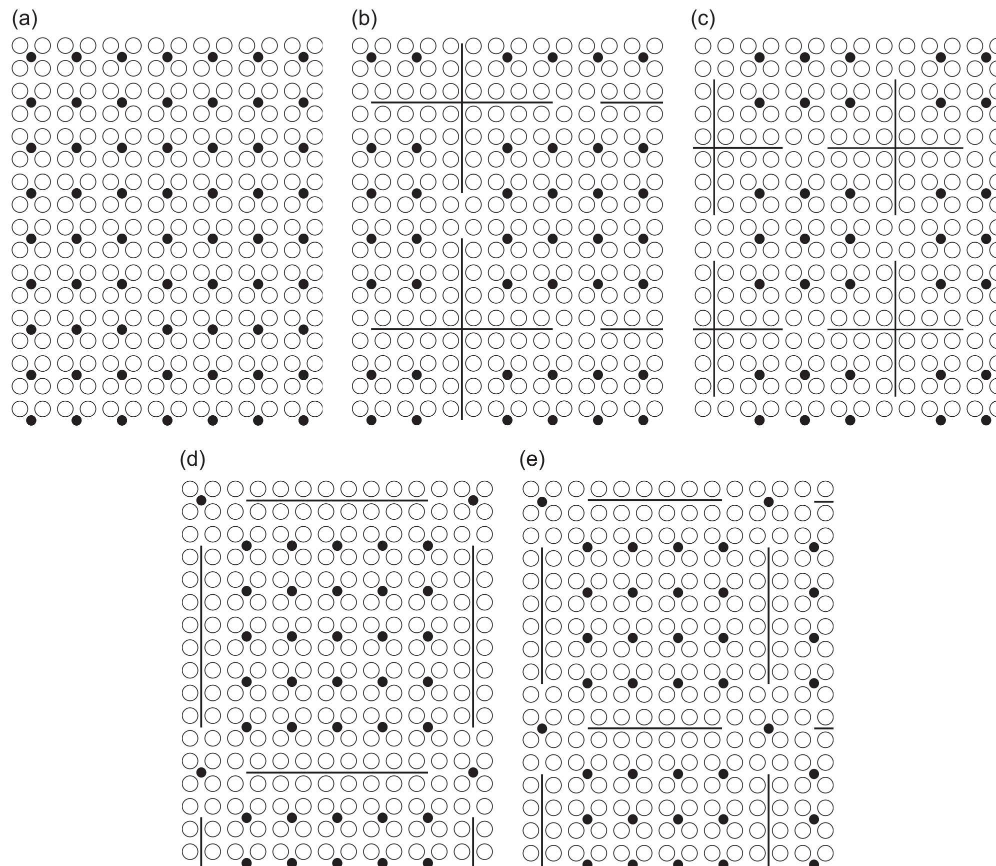

Fig. 6. Details of SU-8 structures in the chip's active area reducing the radial stress in the aluminium layer. The open circles represent the grid holes (55 μm pitch), the closed circles SU-8 pillars like in the current design (a). The crosses and lines in (b) and (d) have a length of 440 μm, the crosses and lines in (c) and (e) are 330 μm long. The width for all cross and line structures is 17 μm.

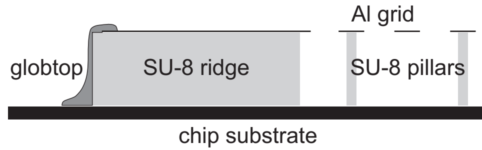

Fig. 7. Illustration of globtop reinforcement of the SU-8 ridges along the grid perimeter.

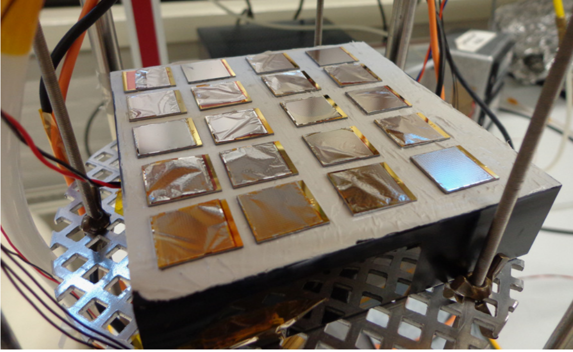

Fig. 8. Picture of modified InGrids after the thermal cycle. Although the grids as a layer are intact, the underlying SU-8 ridges have delaminated. Only the devices with reinforced grid edges are undamaged.

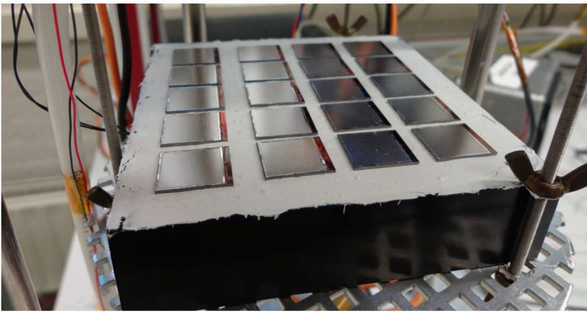

Fig. 9. Picture of the final batch of samples after the thermal cycle. The fixation of the dyke with the help of globtop as well as the improved thermal contact resulted in undamaged InGrids after this thermal cycle.

Fig. 10. Microscope image of the SU-8 structures used for the shear test. These structures serve as alignment markers during the wafer post-processing. Note the SiRN layer (red) extending under the markers on the left chip. The adhesion there is a lot stronger than on the gold layer on the right. Also visible are the different support ridge layouts. (For interpretation of the references to colour in this figure caption, the reader is referred to the web version of this paper.)

for delamination on gold, as measured on 12 samples, amounts to 4.02(117) g before, and 2.69(86) g after the thermal cycle. For SU-8 structures on SiRN, the values are 15.45(347) g and 7.95(481) g, respectively. We find that thermal cycling significantly reduces the adhesion of SU-8 on its substrate. In accordance with earlier studies [10], the results show a stronger adhesion between SU-8 and SiRN than between SU-8 and gold.

5. Functional test of prototypes

Although we use dummy chips rather than real pixel readout chips, the metal layer on the dummy substrate allows high voltage biasing of the structure to enforce gas gain. This allows the recording of signals by ionizing radiation in a suitable gas, be it without position information. The pulse height spectrum of monochromatic X-rays from an ^{55}Fe source was recorded in this manner, using the setup shown in Fig. 11.

To this purpose the chips of three distinct layouts are glued on a PCB with contact lines and connection pins to connect the anode, the grid and the cathode to a power supply and the readout. The drift chamber consists of a thin glass-epoxy frame of 5 mm height, with gas tubes glued into one of its walls. Copper-cladded Kapton foil forms the cathode. A chromium foil between drift chamber and the source absorbs the K_β line of ^{55}Fe at 6.5 keV. The gas tubes are connected to a flow controller supplying the Ar/iC_4H_{10} 90/10 mixture.

The high voltage supplied to the grid is $V_{grid} = 370$ V, and the drift field between grid and cathode is kept constant at $E_{drift} = 300$ V/cm. The anode is connected to ground potential. The signal is read out via a high voltage pin, decoupled from the high voltage supply by a 100 nF capacitor, and shaped by a preamplifier. A closed metal box and ferrite rings around the signal cables minimize the pick-up noise. The gain of the amplifier is adjusted to use the full range of the ADC to record the pulse height spectrum of the signals.

The obtained spectra clearly show the photopeak and the escape peak, see Fig. 12 for a sample spectrum. To determine the energy resolution we fit a function that is the sum of three Gaussians and a linear function:

$$f(x) = \underbrace{A\exp\left(-\frac{(x-\mu_{esc})^2}{2\sigma_{esc}^2}\right)}_{\text{escape peak}} + \underbrace{B\exp\left(-\frac{(x-\mu_\alpha)^2}{2\sigma_\alpha^2}\right)}_{\text{photopeak},K_\alpha} + \underbrace{C\exp\left(\frac{-(x-\mu_\beta)^2}{2\sigma_\beta^2}\right)}_{\text{photopeak},K_\beta} + D + Ex. \quad (1)$$

The third Gaussian is for taking into account the suppressed (but remaining) K_β line of ^{55}Fe at 6.5 keV. The peak position μ_β and the standard deviation σ_β of the third Gaussian are not free parameters, but fixed with respect to $\mu_\alpha - \mu_{esc}$ and σ_α, respectively.[4] From the obtained K_α standard deviation σ_α we determine the energy resolution ΔE according to

$$\Delta E = \text{FWHM} = 2\ln 2 \times \sigma_\alpha \approx 2.35\sigma_\alpha. \quad (2)$$

Table 2 compares the energy resolution of the spectra of the different samples. The SU-8 design with the best energy resolution is the reference layout, followed by the design with lines before the one that has crosses next to the pillars. We can conclude that additional SU-8 structures influence the detector's energy resolution where cross structures disturb the avalanches more than lines.

To determine the reason for the loss in energy resolution we record a multitude of pulse height spectra in short consecution. For this purpose we use the detector with sample 2 where we found the worst energy resolution since any effect will be most visible with that detector. This measurement is divided into three time series. The second series was taken after leaving the high voltage off for about 5 h. The third series started on the following day.

[4] The DC offset of the used ADC is not fixed to zero. That is why we use μ_{esc} as an absolute fit parameter and we neglect the K_β contribution to μ_{esc}. Overestimating μ_{esc} in this way leads to an energy resolution that is systematically overestimated by $< 0.25\%$.

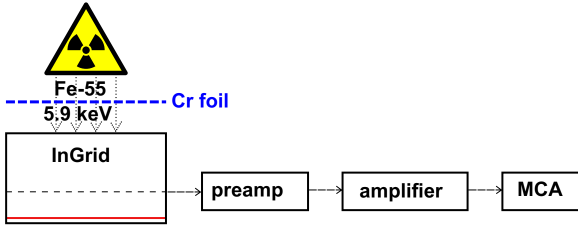

Fig. 11. Schematic of the readout chain for the gaseous detector made from modified grid structures. A chromium foil largely absorbs the K_β line of ^{55}Fe at 6.5 keV. The positive signal induced on the grid is shaped by the preamplifier and amplified by an Ortec 572 amplifier. An Amptek Pocket MCA8000A multi-channel analyser records the pulse height spectrum of the signals.

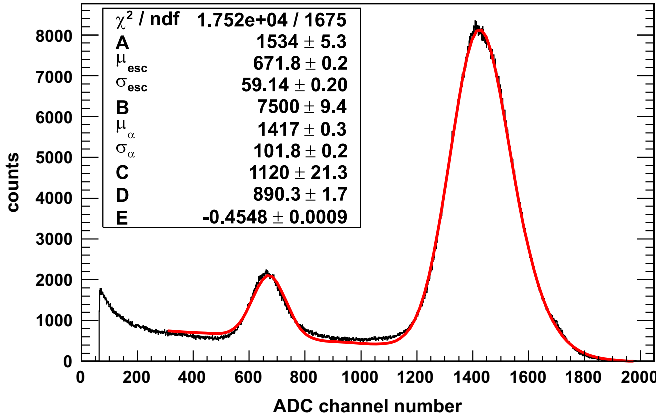

Fig. 12. Pulse height spectrum of an ^{55}Fe source recorded with a prototype detector in Ar/iC_4H_{10} 90/10. Note that the ADC threshold is chosen higher than the baseline. Moreover, the DC level of the amplifier's output is slightly negative. This is compensated by using the known relative distance between the photo- and the escape peak.

Table 2
Energy resolution at the photopeak of ^{55}Fe (5.9 keV) and the measured grid height difference Δh of the tested modified InGrid designs.

Sample	SU-8 layout	$\Delta E/E$ (%)	Δh (μm)
1	Reference (Fig. 6a)	14.53(2)	1.0
2	Crosses (Fig. 6b)	15.95(3)	2.6
3	Lines (Fig. 6d)	15.38(1)	1.6

We find that the energy resolution is not time-dependent: apart from a small decrease during the first 5 min it does not show a significant trend. We do observe, however, that the position of the photopeak moves to lower values in terms of ADC channels, see Fig. 13. The pulse height hence decreases over time, meaning that less charge is moving within the amplification region (in form of an avalanche). The subsequent series show a similar behaviour for the initial period when the SU-8 of the detector is not yet charged up. This indicates that the SU-8 is indeed charging up over time and the less SU-8 material is in the amplification gap, the more stable the gas gain is. This latter finding is further supported by measurements of the grid height profile, see Fig. 14, using a white light interferometer.[5] The added SU-8 structures lift the grid about up to 2.6 μm, see the last column of Table 2. This means that not all grid holes are at the same height above the chip. The resulting gas gain fluctuations lead to a reduced energy resolution.

[5] The surface is measured with a Bruker Contour GT-I at the MESA+ Nanolab, University of Twente. The analyser uses vertical scanning interferometry and pixel intensity measurement to determine relative heights.

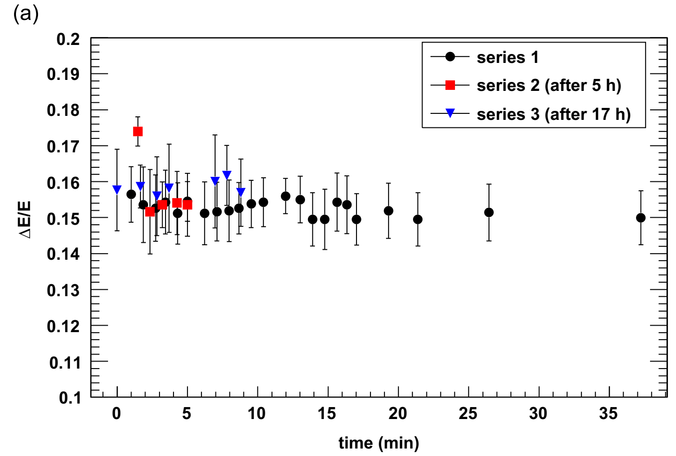

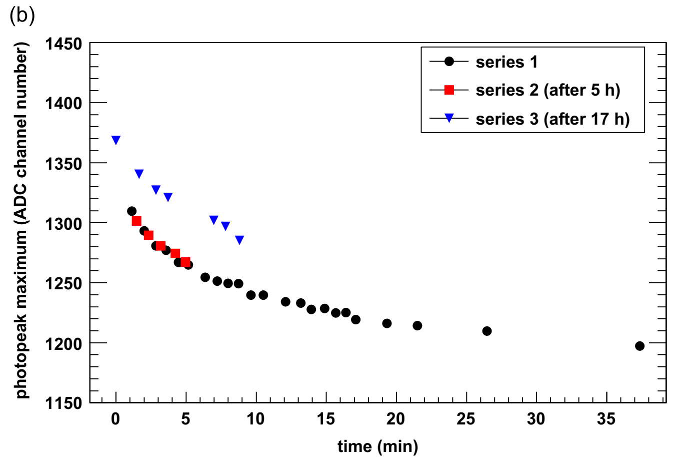

Fig. 13. Time dependence of the energy resolution (a) and the peak position (b). While the energy resolution does not decrease notably, the position of the photopeak (in ADC channels) shifts towards lower values, so less charge is being collected. This indicates that parts of the avalanche are being quenched by charged-up SU-8 structures. The second and third time series were taken after breaks of 5 and 17 h, respectively. They show the same initial behaviour of a yet uncharged detector.

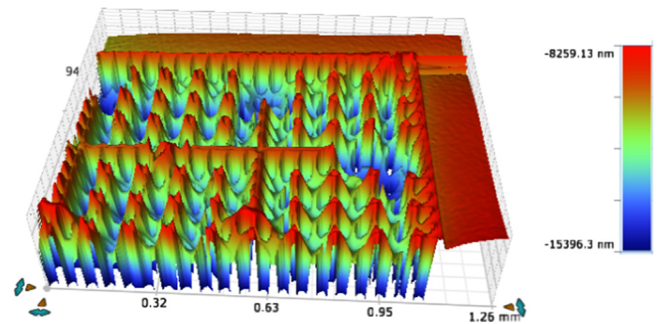

Fig. 14. Detailed view of the measured grid height profile with added SU-8 crosses. The height of the grid holes around this structure is increased by about 2 μm, reducing the amplification field underneath.

6. Conclusions

GridPix emulating test samples were successfully cooled down to −130 °C. A low cool-down rate and thermal contact with the environment were shown to be of critical importance. Only globtop-reinforced grids provide the desired stability of the GridPix structure. This cannot be achieved through a dedicated SU-8 pattern alone.

Instead the special reinforcing SU-8 structures tested in this work have a negative influence on the energy resolution of the GridPix detector; and having no decisive effect on the mechanical stability, they are better avoided.

Acknowledgements

We thank Richard Rosing for the FEM simulations. We also acknowledge the tremendous help of Filippo Resnati and Devis Lussi of the ETH Zurich group of the ArDM experiment during the operation of GridPix in their detector.

References

[1] V.M. Blanco Carballo, et al., IEEE Electron Device Letters 29 (6) (2008) 585.
[2] Y. Giomataris, et al., Nuclear Instruments and Methods in Physics Research Section A 376 (1) (1996) 29.
[3] X. Llopart, et al., IEEE Transitions on Nuclear Science NS-49I (5) (2002) 2279.
[4] X. Llopart, et al., Nuclear Instruments and Methods in Physics Research Section A 581 (2007) 485.
[5] W.J.C. Koppert, et al., Nuclear Instruments and Methods in Physics Research Section A 732 (2013) 245.
[6] L. Baudis, for the DARWIN consortium, Dark Matter Wimp Search with Noble Liquids, 2010, arXiv:1012.4764.
[7] R. Schön, Development of liquid xenon detector technology for dark matter searches (Ph.D. thesis), Universiteit van Amsterdam, in preparation.
[8] R. Schön, et al., Nuclear Instruments and Methods in Physics Research Section A 771 (2015) 74.
[9] S. Bystrova, et al., Microelectronic Engineering 84 (5–8) (2007) 1113.
[10] V.M. Blanco Carballo, et al., Microelectronic Engineering 86 (2009) 765.
[11] A. Badertscher, et al., Nuclear Instruments and Methods in Physics Research Section A 641 (2011) 48.
[12] Dymax Website, Dymax 9001-E-v3.1 UV-Curable Encapsulant ⟨http://www.dymax.com/index.php/adhesives/products/9001-e-v31⟩.
[13] 3DS Website, Abaqus Finite Element Analysis Software ⟨http://www.3ds.com/products-services/simulia/products/abaqus⟩.